Mechanical phase matching of birefringent non-linear crystals

Loïc Deyra, François Balembois, André Guilbaud, Philippe Villeval, Patrick Georges

Mechanical phase matching of birefringent non-linear crystals

Loïc Deyra,[1,*] François Balembois,[1] André Guilbaud,[1] Philippe Villeval,[2] and Patrick Georges[1]

[1] *Laboratoire Charles Fabry, Institut d'Optique, CNRS, Univ Paris-Sud, 91127 Palaiseau, France*
[2] *Cristal Laser, ZAC du Breuil – 32, rue Schumann 54850 Messein- France*
[*] *loic.deyra@institutoptique.fr*

Abstract: Second-order nonlinear processes such as second harmonic generation or parametric amplification have found numerous applications in the scientific and industrial world, from micromachining to petawatt laser facilities. These nonlinear interactions are mostly carried out in birefringent crystals because of their low cost and the possibility to operate at high powers Phase-matching configurations in birefringent crystals are determined by their refractive indexes. Here, we show that an important mechanical stress can be used to significantly change the phase-matching properties of a birefringent crystal. As an example, we demonstrate the shift of second harmonic non-critical phase matching wavelength of LiB3O5 (LBO) crystal at room temperature from 1200 nm to 1120 nm by applying compressive forces up to 100 MPa. We believe that this mechanical phase matching can be used as an additional degree of freedom to optimize nonlinear optical frequency mixing geometries.

References and links

1. G. D. Boyd, A. Ashkin, J. M. Dziedzic, and D. A. Kleinman, "Second-Harmonic generation of Light with Double Refraction," Phys. Rev. **137**(4A), 1305–1320 (1965).
2. G. Cerullo and S. De Silvestri, "Ultrafast optical parametric amplifiers," Rev. Sci. Instrum. **74**(1), 1–18 (2003).
3. S. Demmler, J. Rothhardt, A. Zaïr, M. Krebs, S. Hädrich, L. Chipperfield, J. Limpert, and A. Tünnermann, "Towards isolated attosecond pulses at megahertz repetition rates," Nat. Photonics **7**(7), 555–559 (2013).
4. M. D. Perry, D. Pennington, B. C. Stuart, G. Tietbohl, J. A. Britten, C. Brown, S. Herman, B. Golick, M. Kartz, J. Miller, H. T. Powell, M. Vergino, and V. Yanovsky, "Petawatt laser pulses," Opt. Lett. **24**(3), 160–162 (1999).
5. J. J. Chang, B. E. Warner, E. P. Dragon, and M. W. Martinez, "Precision micromachining with pulsed green lasers," J. Laser Appl. **10**(6), 285 (1998).
6. A. Kokh, N. Kononova, G. Mennerat, P. Villeval, S. Durst, D. Lupinski, V. Vlezko, and K. Kokh, "Growth of high quality large size LBO crystals for high energy second harmonic generation," J. Cryst. Growth **312**(10), 1774–1778 (2010).
7. T. Schreiber, H. Schultz, O. Schmidt, F. Röser, J. Limpert, and A. Tünnermann, "Stress-induced birefringence in large-mode-area micro-structured optical fibers," Opt. Express **13**(10), 3637–3646 (2005).
8. Z. Y. Yu, F. Xu, F. Leng, X. S. Qian, X. F. Chen, and Y. Q. Lu, "Acousto-optic tunable second harmonic generation in periodically poled LiNbO3," Opt. Express **17**(14), 11965–11971 (2009).
9. Z. Ma, K. Wu, R. Sa, K. Ding, and Q. Li, "Strain-induced improvements on linear and nonlinear optical properties of SrB4O7 crystal," AIP Adv. **2**(032170), 1–6 (2012).
10. C. Chen, Y. Wu, A. Jiang, B. Wu, G. You, R. Li, and S. Lin, "New nonlinear-optical crystal: LiB305," J. Opt. Soc. Am. B **6**(4), 616–621 (1989).
11. I. I. Zubrinov, V. K. Sapozhnikov, N. A. Pylneva, and V. V. Atuchin, "Elastic and elastooptic properties of LiB3O5," Ceram. Int. **30**(7), 1675–1677 (2004).
12. I. P. Shakhverdova, P. Paufler, R. S. Bubnova, S. K. Filatov, Levin, and D. C. Meyer, "Mechanical properties of single crystalline and glassy lithium triborate," Cryst. Res. Technol. **43**(4), 339–349 (2008).
13. J. E. Marion, "Appropriate use of the strength parameter in solid-state slab laser design," J. Appl. Phys. **62**(5), 1595–1604 (1987).
14. T. Ukachi, R. J. Lane, W. R. Bosenberg, and C. L. Tang, "Measurements of non-critically phase-matched second-harmonic generation in a LBO crystal," Appl. Phys. Lett. **57**(10), 980–982 (1990).

15. W. Koechner, “Rupture stress and modulus of elasticity for Nd: YAG crystals,” Appl. Phys., A Mater. Sci. Process. **280**, 279–280 (1973).
16. R. Feldman, Y. Golan, Z. Burshtein, S. Jackel, I. Moshe, A. Meir, Y. Lumer, and Y. Shimony, “Strengthening of poly-crystalline (ceramic) Nd:YAG elements for high-power laser applications,” Opt. Mater. **33**(5), 695–701 (2011).

1. Introduction

Second-order nonlinear processes such as second harmonic generation [1] or parametric amplification [2] have found numerous applications in the scientific and industrial world, from micromachining to petawatt laser facilities [3–5]. These nonlinear interactions are mostly carried out in birefringent crystals because of their low cost and the possibility to operate at high powers [6]. In a χ^2 interaction such as second harmonic generation (SHG), two propagating waves with different frequencies must experience the same phase shift in order to reach high conversion efficiencies. Birefringent phase matching (BPM) uses the anisotropy of a crystal to match the phase velocities of both waves during propagation. The wavelength range that can be covered for a given interaction depends on the crystal refractive indices. Theses indices can be changed by cutting the crystal at specific angles with respect to the crystal axes. This method, usually called angle phase matching or critical phase matching, allows a broad range of wavelengths to be phase-matched. The crystal operating temperature can also be changed to adjust the phase matching wavelength (temperature phase matching).

Here, we propose to use the elasto-optic effect induced by a strong mechanical force to change the phase matching properties of a birefringent crystal: we denote this method as mechanical phase matching.

The refractive index change of a material when stressed (elasto-optic effect) is commonly used in a variety of optical applications such as acousto-optic (AO) devices or polarization maintaining optical fibers [7]. While this effect has been considered theoretically to tune a SHG signal with an AO modulator [8], or as a way to use isotropic nonlinear crystals in BPM [9], it has never been used experimentally in nonlinear frequency conversion to the best of our knowledge.

2. Theoretical principle

Consider a material under a mechanical stress important enough to distort it.

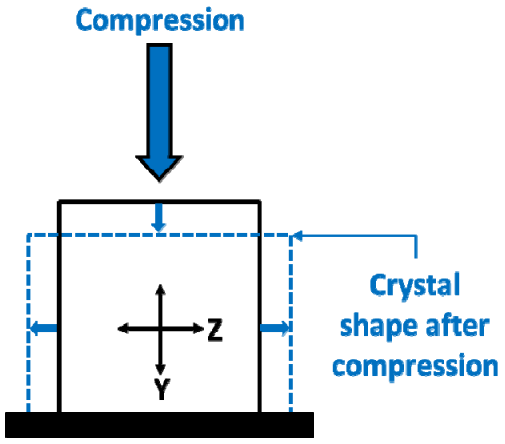

Fig. 1. Illustration of the elasto-optic principle.

In this work, we focus on applying pure compressive forces to crystals cut along their optical axes, for several reasons. First, by stressing crystals along their crystallographic axes, we prevent the appearance of crystal lattice dislocations. Second, we intend to change the

difference between two refractive indices along two axes. Therefore, the optimum use of a compressive force is when it is directed along one of the crystallographic axes.

When a compressive stress is applied to a crystal along direction Y, the material experiences negative strain along the Y-axis; by the Poisson effect, the material then experiences a positive strain along the Z-axis, as illustrated in Fig. 1 (we assume that the crystal is not auxetic). At each location inside the crystal, the local refractive index change is given by:

$$\Delta\left(\frac{1}{n_i^2}\right) = \sum_{j=1..3} \rho_{ij}\varepsilon_j, \tag{1}$$

where n is the refractive index, ρ is the elasto-optic coefficient, ε is the strain, and i and j are indices denoting the direction in space, ranging from 1 to 3. This is a two-dimensional example, but in reality our crystals has 3 dimensions. For now, we use the plane-strain approximation that states that if a material under compressive forces has a dimension longer than the two others, the strain in that longer direction can be neglected.

The experiment is performed using a lithium tetraborate (LiB_3O_5, LBO) crystal [10], a commercial material widely used for frequency conversion to the visible and ultraviolet. LBO has a combination of properties that makes it a good candidate for mechanical phase matching. First, it features a broad transparency range from 160 nm to 2 μm, but a low birefringence that limits the range of fundamental wavelengths that can be frequency-doubled. It exhibits high damage threshold and very good mechanical resistance. Finally, a particularly interesting configuration for LBO is type-I second harmonic generation in non-critical phase matching (NCPM) orientation. In this configuration, both the fundamental and second harmonic polarization vectors are aligned with crystallographic axes, increasing the interaction length and final conversion efficiencies. We consider second harmonic generation in LBO crystal cut at theta = 90° and phi = 0°, also called X-cut crystal. In this configuration, the fundamental wave is polarized along the Z-axis and the frequency-doubled wave is polarized along the Y-axis (Type-I SHG). We focus on reducing the NCPM wavelength of X-cut LBO. The phase matching condition can be written as:

$$n_z(\omega) = \mathrm{n}_y(2\omega), \tag{2}$$

where n_Z and n_Y are the refractive indices along the Z and Y axes, and ω the angular frequency of the fundamental wave. Combined with Sellmeier equations taken from [9], we compute Δn = ny(2ω)-nz(ω) as a function of ω, displayed as the solid blue curve in Fig. 2. We point out that we use the term “birefringence” for a refractive index difference calculated at two different wavelengths, which is different from the standard birefringence term. A fundamental wavelength can be phase-matched for NCPM SHG when the condition Δn = 0 is satisfied, illustrated by the dotted horizontal red line in Fig. 2. At room temperature, NCPM SHG can be achieved around 1200 nm. The range of wavelengths that can be converted in this configuration is limited by the oven/cooling system capacity. If we apply a stress that decreases the total birefringence Δn, the solid curve shifts downwards, and intersects the phase-matching line at a lower wavelength: the NCPM wavelength is thus lowered. The sign of the induced birefringence depends on the combination of shear and compression stresses. Considering the elasto-optic coefficient sign in the compliance matrix in LBO [11], a positive stress σ_Y (from a compressive force) along the Y axis reduces the birefringence, while the opposite effect can be obtained by applying a stress σ_Z along the Z axis (Fig. 2).

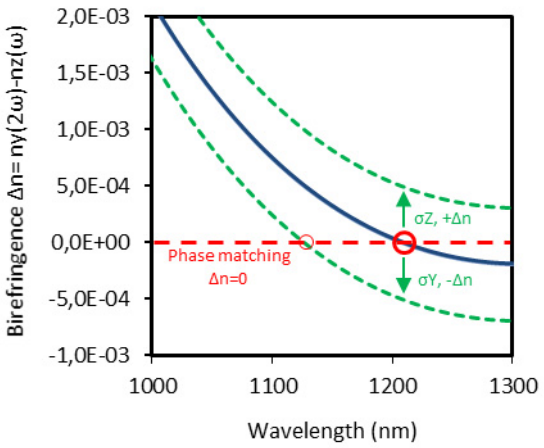

Fig. 2. Influence of birefringence change on NCPM wavelength; (solid curve) birefringence for NCPM SHG in LBO cut at $\theta = 90°$, $\varphi = 0°$ at ambient temperature; (Green dotted lines) birefringence change induced by applied stress; (Red dotted line) Phase matching condition.

The change of phase-matching wavelength thus depends on the compression force, induced stress and birefringence. Finite element simulations can be used to assess these quantities. However, such models are fundamentally limited by the uncertainty on elastic and elasto-optic coefficients of LBO: a rough estimate was reported in a single reference [11]. Moreover, the predictive character of such simulations is limited in practice, since the compression system itself and the crystal surface quality play a key role. For example, if the applied stress is not perfectly uniform, local stress points can cause early crystal fracture. Therefore, we carried out a first experiment in order to determine the strain uniformity, and the crystal mechanical damage threshold, with a particular attention to the interface between the crystal and the compression mount.

3. Mechanical study

The compression mount is displayed in Fig. 3. It was mechanically designed to apply a pure compression force and avoid parasitic torsion effects: a single M6 screw applies a torque to a translating element locked in rotation. The mechanical parts are made of 35NCD16 hard steel to avoid deformation of the mount itself. The torque applied to the screw is measured using a torque measurement screwdriver. The relation between applied torque and applied compressive force is measured by a compression sensor located at the crystal position. Compression forces between 0 and 12 kN can be applied with a precision of + –0.1 kN with applied torques between 0 and 10 Nm. The final mechanical element delivering the force has a section of 4x12 mm^2, and its surface is optically polished.

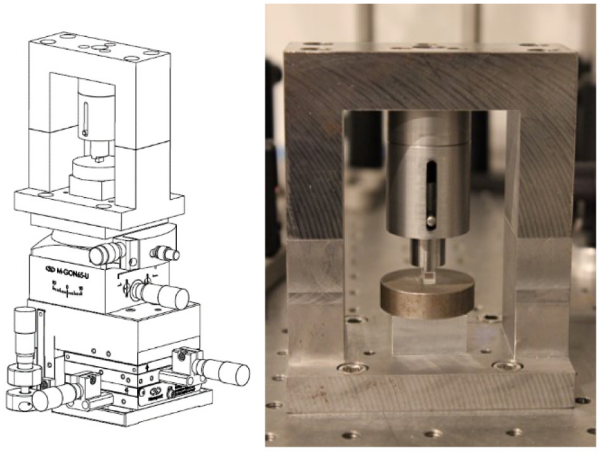

Fig. 3. Scheme and picture of the compression mount.

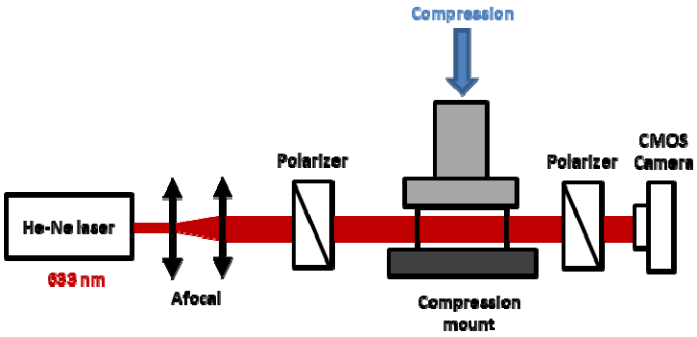

Fig. 4. Experimental setup for stress-induced birefringence analysis.

We investigate the strain uniformity by inserting the constrained crystal in a strain-optical analysis bench as depicted in Fig. 4. The output beam from a He-Ne laser at 633 nm is collimated and sent into the crystal, placed between crossed polarizers. The crystal axes are oriented at 45° with respect to the crossed polarizers. We observe interference patterns with a CCD camera. Fringes appear when elasto-optic induced local index changes modify the polarization of the transmitted light. Experimental results are displayed in Fig. 5.

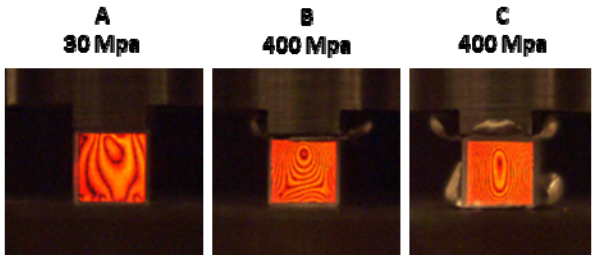

Fig. 5. Stress-induced birefringence measurements depending on the crystal-mount interface. (A) Without indium foil; (B) With indium foil on top surface only; (C) With indium foil on both surfaces. Crystals are constrained along the Z axis.

They show interference patterns obtained for LBO crystals cut along the X axis constrained along their Z axis with a force just below fracture. In the first configuration (Fig. 5(A)), the crystal is constrained without any interface material. The strain uniformity is very

poor, and cracks on the bottom surface quickly appear. The maximum applied pressure in this case is 30 MPa. We then use indium as an interface material to increase strain uniformity on crystal facets. Indium is a very soft material that can wet solid surfaces, and thus helps smoothing possible defects between the crystal and the compression element. When a 200 µm indium foil is inserted between the top crystal facet and the compressive element, the fracture threshold increases to 400 MPa. The bottom corners of the crystal suffer from increased strain because the bottom surface is unable to extend and move. If a second indium foil is inserted under the crystal, the induced birefringence becomes highly uniform, and the fracture threshold remains at 400 MPa (Fig. 5(C)). In this case the fringes start to appear at the crystal center, where the stress is maximum. This section area is approximately one by two millimeters, large enough to focus a laser beam through. The fringe pattern is formed by the stress gradient between the crystal center and the edges. Indeed, the material can expand at its edges, which helps relaxing the applied stress.

We also constrained LBO crystals along their Y axis. In this case, the fracture threshold decreases to 100 MPa, because of the elasto-optic anisotropy of LBO [11]. The fracture threshold results are summarized in Fig. 6.

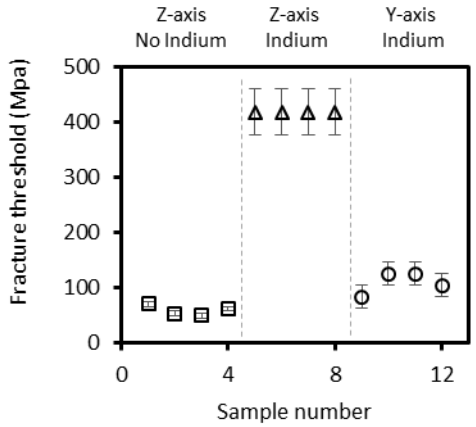

Fig. 6. Damage threshold results. Samples 1 to 4: constraint along Z-axis, without indium; Samples 5 to 8: constraint along Z-axis, with indium; Samples 9 to 12: constraint along Y-axis, with indium.

The theoretical fracture limit of a material is sometimes given as one tenth of Young modulus: in the case of LBO, with a Young modulus of about 140 GPa [12], the fracture threshold should be 14 GPa. This fracture threshold corresponds to the force required to break atomic bonds. In practice, the fracture threshold is often one to two orders of magnitude below this estimate [13]. The damage threshold is actually determined by the rate at which a pre-existing crack grows inside the material. It is thus highly dependent on crystal surface quality (planarity and roughness) and stress uniformity.

3. Second harmonic generation experiment

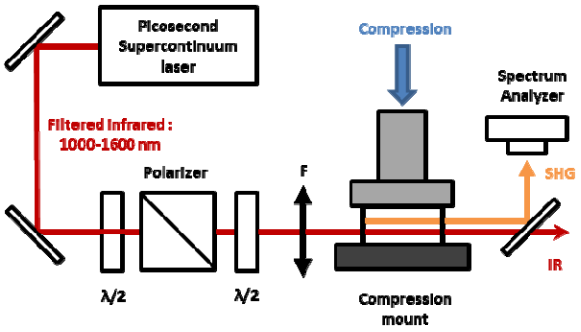

Fig. 7. Experimental setup for second harmonic generation.

We now focus on a second harmonic generation experiment with a uniformly constrained crystal. The experimental setup is displayed in Fig. 7. In order to observe phase matching wavelength change over a broad range, we use a supercontinuum fiber laser source, emitting up to 4 W at 40 MHz from 400 nm to 2 µm with a pulse width of 5 ps. This signal is filtered using dichroic mirrors as shown in Fig. 8.

The filtered beam from 1000 to 1300 nm is focused inside the nonlinear crystal center zone at a beam focus diameter of 50 µm. As the spectrum is extremely broad, multiple sum-frequency generation processes can occur, and the resulting spectral width of the second harmonic signal does not correspond to the spectral acceptance of the conversion process. Therefore, in order to avoid parasitic sum frequency processes, a spectral filtering is needed. We used the chromatic aberration of a standard lens: each spectral component is located at a different place along the propagation axis, thus limiting the interaction between different wavelengths. The conversion efficiency cannot be measured with this set-up, as it is designed only to characterize the phase-matching wavelength shift. The second harmonic center wavelength was measured with a visible spectrometer (190-600 nm, resolution + –0.3 nm). We ensure that the nonlinear crystal is properly aligned at the NCPM angle by alignment of the frequency doubled signal reflection on the crystal output face (perpendicular to the X axis) with the input IR beam. As mentioned above, only the center wavelength of the measured SHG spectrum is accurate. In our experiment, we want to lower the NCPM wavelength.

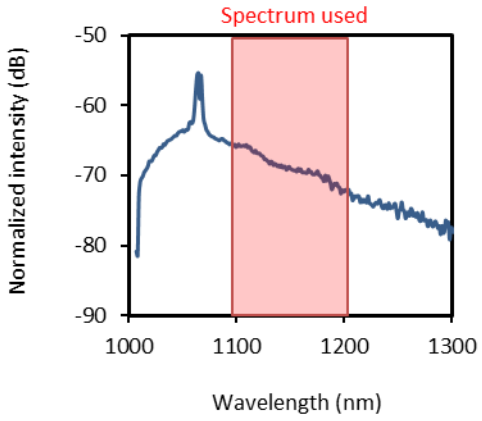

Fig. 8. Spectral distribution of the supercontinuum average power.

Based on the curves of Fig. 2, the LBO crystal is constrained along the Y-axis: and the refractive index difference Δn decreases. We applied up to 100 MPa on the crystal surface, corresponding to the crystal fracture threshold. The results are shown in Fig. 9. The frequency-doubled wavelength shifts from 1200 nm to 1120 nm. Displayed spectra are normalized, because the fundamental laser spectrum is not constant over 1100 – 1200 nm. The wavelength shift is stable over several hours. At strong stress values, ripples appear in the frequency doubled spectrum. This feature is not fully understood yet, but we attribute it to the refractive indexes along Y and Z axis being non-uniform along the longitudinal direction (X-axis in this case): the propagating wave would then see an index gradient, resulting in multiple phase-matching wavelengths.

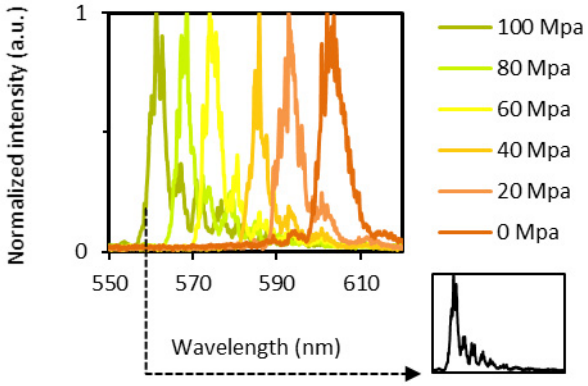

Fig. 9. Second harmonic spectrum as a function of stress magnitude; insert shows spectrum ripples at 100 MPa.

Finally, the measured phase matched wavelength shift can be related with induced birefringence measurements realized using the setup presented in Fig. 4.

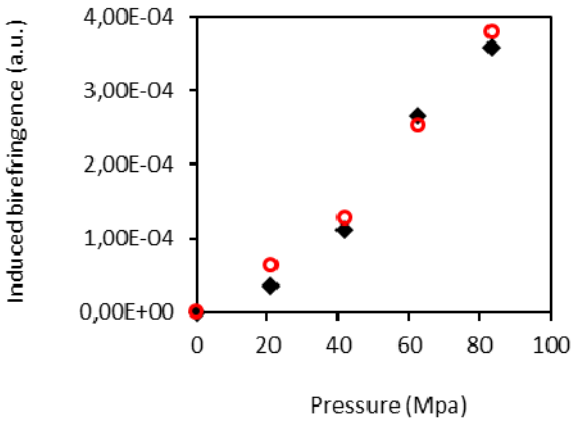

Fig. 10. Induced birefringence as a function of applied pressure. (Black diamond) retrieved from SHG wavelength shift; (Red circles) retrieved from number of fringes using the crossed polarizers setup.

While they measure two different kind of birefringence, we can neglect the dispersion and see if the orders of magnitude are comparable. First, using Fig. 2, the phase matched wavelength shift is translated into birefringence change. Second, for each pressure value, we evaluate the induced birefringence by counting the number of fringes appearing at the crystal center in the experimental setup of Fig. 4.

Each fringe corresponds to an induced relative phase of 2π between orthogonal polarizations of the He-Ne beam at 633 nm. In terms of birefringence, a fringe therefore corresponds to $\Delta n = \lambda/e = 6.33 \times 10^{-5}$, where λ is the He-Ne wavelength and e the crystal length. The results are presented in Fig. 10. We could not go beyond 80 MPa in this measurement because of crystal fracture. Both measurements concur in term of induced birefringence value.

4. Conclusion

We demonstrate the change of NCPM wavelength of a birefringent crystal by applying a mechanical force. This wavelength shift is only limited by the material damage threshold. It can be compared with NCPM wavelength shifts induced by temperature in LBO [14]: by mechanical constraint, we have shifted the NCPM wavelength by an amount equivalent to a temperature increase of 60°C. In this experiment, no particular surface treatment has been applied on constrained facets. Yet, fractures studies on Nd:YAG rods have shown that optical polishing [15] and chemical etching [16] can improve a crystal fracture limit by an order of magnitude. We can therefore expect to extend the phase-matching range much further.

Mechanical phase matching (MPM) a unique passive technique for phase matching tuning: once the stress is applied, no additional energy is required to maintain the system in its state. Moreover, it only requires mechanical elements and could potentially be designed into a very cheap system. Used for SHG, the phase-matching wavelength can be changed without introducing walk-off, which reduces conversion efficiencies and degrades final beam quality. We anticipate that MPM could be applied to a wide range of nonlinear processes that require birefringence change.

Acknowledgments

This work is funded by French agencies ANR (Agence Nationale de la Recherche) and DGA (Direction Générale de l'Armement) under contract ANR −13-ASTR-0020-01.